Pflugers Arch - Eur J Physiol (2014) 466:477–490
DOI 10.1007/s00424-013-1317-x

Relative contribution of different transmembrane segments to the CFTR chloride channel pore

Wuyang Wang · Yassine El Hiani · Hussein N. Rubaiy · Paul Linsdell

Received: 7 May 2013 / Revised: 18 June 2013 / Accepted: 18 June 2013 / Published online: 20 August 2013

Abstract The membrane-spanning part of the cystic fibrosis transmembrane conductance regulator (CFTR) Cl^- channel comprises 12 transmembrane (TM) α-helices, arranged in 2 symmetrical groups of 6. However, those TMs that line the channel pore are not completely defined. We used patch clamp recording to compare the accessibility of cysteine-reactive reagents to cysteines introduced into different TMs. Several residues in TM11 were accessible to extracellular and/or intracellular cysteine reactive reagents; however, no reactive cysteines were identified in TMs 5 or 11. Two accessible residues in TM11 (T1115C and S1118C) were found to be more readily modified from the extracellular solution in closed channels, but more readily modified from the intracellular solution in open channels, as previously reported for T338C in TM6. However, the effects of mutagenesis at S1118 (TM11) on a range of pore functional properties were relatively minor compared to the large effects of mutagenesis at T338 (TM6). Our results suggest that the CFTR pore is lined by TM11 but not by TM5 or TM7. Comparison with previous works therefore suggests that the pore is lined by TMs 1, 6, 11, and 12, suggesting that the structure of the open channel pore is asymmetric in terms of the contributions of different TMs. Although TMs 6 and 11 appear to undergo similar conformational changes during channel opening and closing, the influence of these two TMs on the functional properties of the narrowest region of the pore is clearly unequal.

W. Wang · Y. El Hiani · H. N. Rubaiy · P. Linsdell (✉)
Department of Physiology and Biophysics, Dalhousie University, PO Box 15000 Halifax, Nova Scotia B3H 4R2, Canada
e-mail: paul.linsdell@dal.ca

Present Address:
W. Wang
Department of Molecular, Cellular and Developmental Biology, University of Michigan, Ann Arbor, MI, USA

Keywords Chloride channel · Cystic fibrosis transmembrane conductance regulator · Ion channel pore · Permeation · Site-directed mutagenesis · Substituted cysteine accessibility

Introduction

Cystic fibrosis is caused by genetic mutations that result in loss of function of the cystic fibrosis transmembrane conductance regulator (CFTR) protein [27]. CFTR is a member of the ATP-binding cassette (ABC) family of membrane proteins that functions as a phosphorylation-regulated, ATP-gated Cl^- channel [12]. In common with other ABC proteins, CFTR has a modular architecture, consisting of two membrane-spanning domains (MSDs) each followed by a cytoplasmic nucleotide binding domain (NBD). The transmembrane Cl^- channel pore is formed by the two MSDs, each of which contains six transmembrane α-helices (TMs 1–12) [12, 18, 21]. The structure of the MSDs in CFTR has been observed only at low resolution [17, 35]. However, atomic homology models based on the structures of other ABC proteins suggest that a subset of the TMs form a central pore in a symmetrical fashion consistent with the presence of two symmetrical MSDs [7, 31–33, 36]. In fact, due to domain swapping, the MSDs appear to be arranged in two symmetrical "wings," one made up of TMs 1, 2, 9, 10, 11, 12, and the other TMs 3, 4, 5, 6, 7, 8 [17]. These model structures all suggest crucial pore-lining roles for TMs 6 and 12, with possible supporting roles of symmetrical TM pairs 1 and 7, and 5 and 11 [7, 17, 31–33, 36]. These models are therefore quite consistent with functional [18, 21, 28] and substituted cysteine accessibility mutagenesis (SCAM) evidence [2–5, 9, 10, 13, 33, 34, 44] that TMs 1, 6, 11, and 12 line the channel pore and determine its functional properties. However, the relative positions and alignments of these TMs

in the three-dimensional structure of the pore are only beginning to be investigated experimentally [43, 44, 49]. Furthermore, the potential contribution of other TMs is not known, and as a result it is not known how many TMs line the pore. Partial evidence has been put forward in support of a pore-lining role for TM3 [1, 33], TM5 [14, 28, 39] and TM9 [33]. Furthermore, if the two TMDs do indeed make symmetrical contributions to the pore, then the suggested pore-forming roles of TMs 1 and 11 should be reflected in similar contributions by TMs 7 and 5, respectively [7, 17, 31–33].

Uncertainty concerning the identity, relative positions, and relative alignment of different TMs lining the CFTR pore make it difficult to describe and understand the three-dimensional organization of functionally important pore regions such as the outer vestibule [37, 45, 47], narrow region [26, 29, 33], putative channel "gate" [41], and inner vestibule [6, 9, 19, 40, 48, 49]. In many cases, the identity of TM6 residues contributing to these functionally important pore regions has been described, but functionally analogous amino acid residues from other TMs have not been identified [18, 21]. For example, the narrowest part of the pore that might form a "selectivity filter" that discriminates weakly between Cl^- and other small permeant anions is thought to be lined by TM6 residues F337 and T338 [21]. Consistent with this idea, channel functional properties such as single channel conductance and relative permeability of different anions are strongly dependent on the volume of the amino acid side chain present at these two positions [24, 26]. In particular, replacement of T338 with a smaller alanine residue causes (a) an increase in single channel conductance [26], (b) increased permeability of lyotropic anions (those with a low free energy of hydration) such as SCN^- [26, 29] and $Au(CN)_2^-$ [15], (c) altered block of Cl^- permeation by permeant SCN^- and $Au(CN)_2^-$ ions [11, 15, 22], and (d) increased permeability of small organic anions such as acetate, the permeability of which is thought to be limited by steric factors as they pass through the narrow pore region [25, 26]. Overall, the effects of the T338A mutation have been interpreted as reflecting an increase in functional diameter of the narrowest part of the pore [26] and a reduced barrier to the movement of permeant ions inside the pore [11]. However, although other TMs besides TM6 presumably also line the narrow pore region, the effect of mutations at T338 and/or F337 has not been reproduced by mutagenesis of residues from any other TM.

As a complement to earlier SCAM studies on TMs 1, 6, and 12 [8, 34, 44], we have studied the accessibility of cysteines introduced into TMs 5, 7, and 11 to the methanethiosulfonate (MTS) reagent [2-sulfonatoethyl] MTS (MTSES). Whereas cysteines introduced into TMs 5 and 7 do not appear accessible to internal MTSES, several residues in TM11 are accessible to MTSES applied to the inside of the membrane, to the outside, and in some cases to either side. While this pattern of accessibility is similar to that described previously for TM6 [8, 42], comparison of the functional effects of mutations at T338 in TM6 with those at the analogous position in TM11 (S1118) suggest that these two TMs make unequal contributions to the functional properties of the pore. We propose that the CFTR pore is lined by TMs 1, 6, 11, and 12; however, these TMs appear to have distinct roles in determining pore functional properties.

Materials and methods

Experiments were carried out on baby hamster kidney cells transiently transfected with CFTR. In this study, we have used two different human CFTR variants as backgrounds for further mutagenesis: wild type CFTR and "cys-less" CFTR in which all cysteines have been removed by mutagenesis [30] and that also includes a mutation in the first NBD (V510A) to increase protein expression in the cell membrane [20]. Additional mutations were introduced into these two backgrounds using the QuikChange site-directed mutagenesis system (Agilent Technologies, Santa Clara, CA, USA) and verified by DNA sequencing.

Investigation of different TMs by SCAM was guided by current atomic homology models of CFTR's MSD regions (Fig. 1). Previous experiments investigating internal MTSES access to TMs 1, 6, and 12 have allowed functional alignment of these TMs [8, 34, 44]. In particular, alignment of these three TMs around a gate in the pore that regulates access from the cytoplasm suggests that K95 (TM1), V345 (TM6), and S1141 (TM12) are located close together in the pore inner vestibule [8, 34, 44]; this alignment is consistent with current models of the MSDs (Fig. 1) and with disulfide cross-linking experiments [44, 49]. In an attempt to identify those parts of TMs 5, 7, and 11 that might also contribute to this region of the pore, we aligned K95, V345, and S1141 with residues that are predicted by homology models to occupy nearby positions in these other TMs (V317 in TM5; V874 in TM7; F1111 in TM11; Fig. 1). Based on these approximate alignments, we initially mutated 6–9 consecutive residues in each of TM5 (F315-L320), TM7 (F870-L878), and TM11 (I1109-S1115) in a region spanning the putative gate to cysteine in a cys-less CFTR background (Fig. 1d). Based on positive results in TM11 and previous results showing accessibility of the outer part of this TM to extracellular MTS reagents [10], we subsequently extended our cysteine mutagenesis efforts in TM11 to more extracellular residues (Fig. 2c). In some cases, cysteine mutants were combined with the NBD2 mutation E1371Q, which we have used previously to abolish ATP-dependent channel gating

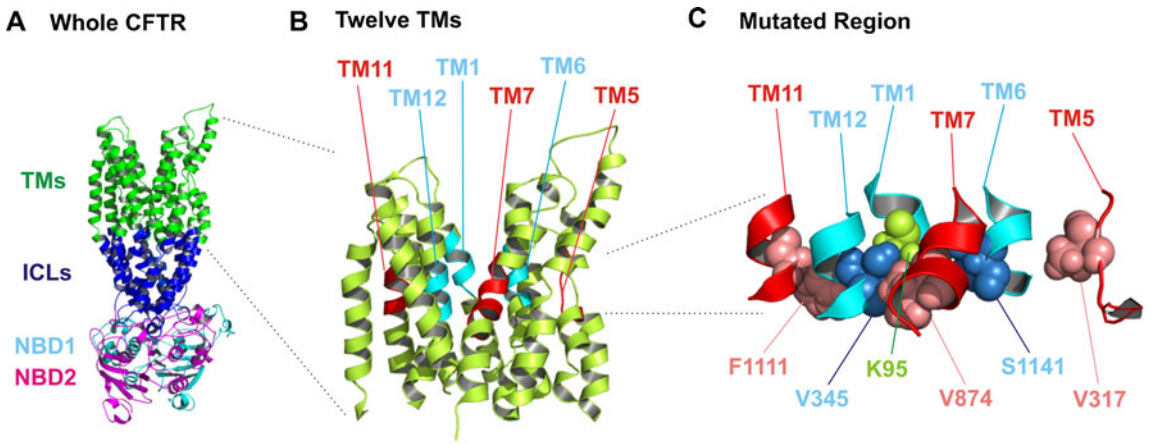

D Alignment of TMs and Residues Selected for Mutation

TM1	*TM6*	*TM12*	*TM5*	*TM7*	*TM11*
P99	S341	M1137	S321	L878	T1115
Q98	F342	N1138	L320	S877	V1114
V97	C343	I1139	F319	A876	A1113
A96	I344	M1140	V318	A875	I1112
K95	V345	S1141	V317	V874	F1111
T94	L346	T1142	F316	E873	F1110
V93	R347	L1143	F315	A872	I1109
E92	M348	Q1144	G314	L871	V1108
G91	A349	W1145	S313	F870	F1107

Fig. 1 Arrangement of putative pore-forming transmembrane helices in a CFTR homology model, and location of regions selected for SCAM. **a** Atomic homology model of CFTR. *ICLs* intracellular loops. **b** Detail of the TMs, indicating the location of regions selected for SCAM (in *red*), together with aligned regions of TMs 1, 6, and 12 (in *blue*). **c** Detail of the central pore regions selected for SCAM, approximately centered around key pore-lining residues K95 (TM1), V345 (TM6), and S1141 (TM12) and putatively aligned residues V317 (TM5), V874 (TM7), and F1111 (TM11). Based on this alignment, the extent of the regions initially selected for SCAM is indicated in **d**. This alignment is centered around those residues shown in **c**, which are *boxed in black* in **d**. Residues in TMs 1, 6, and 12 that have previously been shown, based on SCAM, to have pore-lining side chains [8, 13, 34, 44], are highlighted in *yellow*. Those residues in TMs 5, 7, and 11 selected for SCAM are boxed in red. Illustrated CFTR models in **a**–**c** were based on coordinates provided by Dalton et al. [7] and visualized using PyMol (Schrödinger, LLC, Portland, OR, USA); other published models give approximately similar relative alignment of the TMs

and so isolate effects of cysteine reactive substances on open CFTR channels [41–43].

Macroscopic and single channel CFTR currents were recorded using patch clamp recordings from inside–out membrane patches excised from BHK cells, except for experiments investigating modification by external MTSES described in Figs. 3 and 4b, which were performed using whole-cell patch clamp recording. For inside–out patch recording, following patch excision and recording of background currents, CFTR channels were activated by exposure to protein kinase A catalytic subunit (PKA; 20 nM) plus MgATP (1 mM) in the intracellular solution. Both intracellular (bath) and extracellular (pipette) solutions were based on one containing (mM): 150 NaCl, 2 $MgCl_2$, 10*N*-tris[hydroxymethyl]methyl-2-aminoethanesulfonate, pH 7.4. For experiments investigating the relative permeabilities of different anions (Figs. 7, 8), internal NaCl was replaced by NaSCN (Fig. 7), or external NaCl was replaced by Na acetate (Fig. 8). Measurement of single channel and macroscopic current amplitudes, and construction of leak-subtracted macroscopic current–voltage relationships were carried out as described previously [49]. The rate of modification of introduced cysteine residues by intracellular MTSES was quantified from the change in macroscopic current amplitude as described in detail recently [41, 42]. Briefly, CFTR current amplitudes were monitored during brief voltage deflections (to ±50 mV) from a holding potential of 0 mV applied every 6 s. The measured time constant of exponential current change (at −50 mV) following MTSES application, τ, was used to calculate the apparent second order reaction rate constant, k, from the equation $k=1/([\text{MTSES}]\tau)$. In some cases, the identity of CFTR currents in inside-out patches was confirmed by their sensitivity to the specific inhibitor $CFTR_{inh}$-172 (5 μM).

Whole cell currents were recorded as described in detail recently [42, 43]. Bath (extracellular) solution contained (mM): 145 NaCl, 15 Na glutamate, 4.5 KCl, 1 $MgCl_2$, 2 $CaCl_2$, 10 HEPES, 5 glucose, pH 7.4, and pipette (intracellular) solution contained (mM): 139 CsCl, 2 $MgCl_2$, 5 EGTA, 10 HEPES, 5 mM glucose, 1 ATP, 0.1 mM GTP, pH 7.2. Following attainment of the whole cell configuration and recording of stable baseline currents, CFTR channels were activated by extracellular application of a cyclic AMP stimulatory "cocktail" containing forskolin (10 μM), 3-isobutyl-1-methylxanthine (100 μM), and 8-(4-chlorophenylthio) cyclic AMP (100 μM).

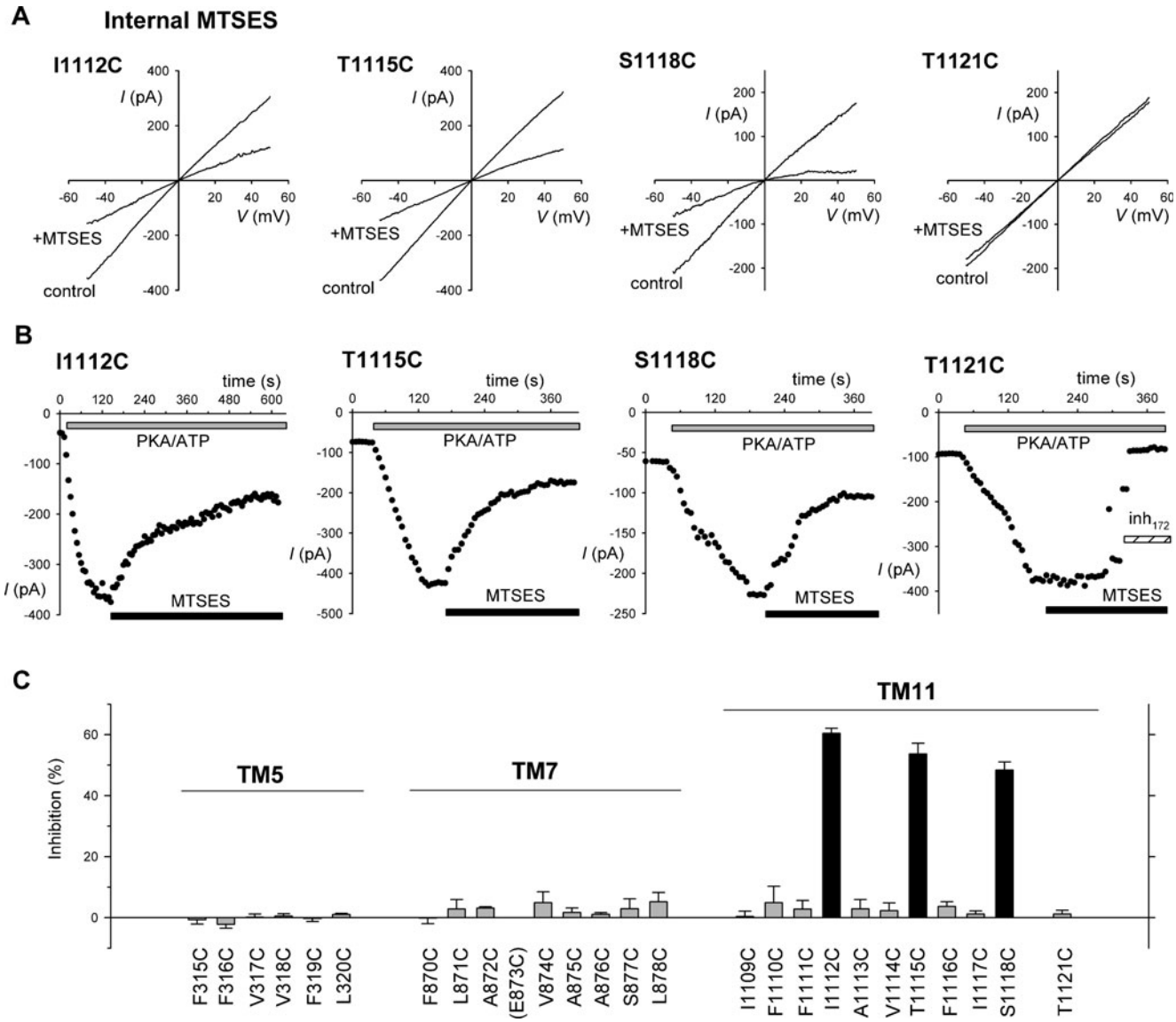

Fig. 2 Modification of cysteine-substituted CFTR mutants by internal MTSES. **a** Example leak subtracted *I–V* relationships for different TM11 cysteine mutants as indicated. In each case, currents were recorded following channel activation with PKA and ATP, before (control) and after addition of 200 μM MTSES to the intracellular solution. **b** Time courses of macroscopic current activation by PKA and ATP (*gray bars*) and effect of MTSES (*black bars*) for these same four membrane patches, monitored at −50 mV. Note that while MTSES caused rapid inhibition of macroscopic current amplitude in T1115C and S1118C, inhibition of I1112C current was much slower (note different time scale for this mutant). MTSES did not affect T1121C currents; however, these were inhibited by $CFTR_{inh}$-172 (5 μM; *hatched bar*). Lack of effect of internal MTSES on cys-less CFTR under identical conditions was shown in our recent publications [8, 34, 44]. **c** Mean effect of internal MTSES on cysteine mutants in TMs 5, 7, and 11. *Black bars* represent a significant difference from cys-less ($P<0.05$); *gray bars* no significant difference. Mean of data from three to six patches. Note that TM11 mutants I1119C and L1120C were not tested since they have previously been shown to be unaffected by extracellular MTS reagents and were therefore described as being non-pore lining [10]. TM7 mutant E873C expression did not yield functional CFTR channel currents in BHK cell patches

Whole cell currents were monitored continuously at a membrane potential of +30 mV. In some cases, the identity of CFTR whole cell currents was confirmed by their sensitivity to the extracellular-active CFTR inhibitor GlyH-101 (50 μM).

Because the properties of T338A-CFTR channels have been investigated in detail previously, simplified protocols were used to facilitate comparison of the effects of the T338A mutation with those of other mutations (Figs. 5, 6, 7, and 8). Single channel recording was used to measure unitary Cl^- conductance under high [Cl^-] conditions (Fig. 5). Block of macroscopic currents by intracellular $Au(CN)_2^-$ ions was used as a measure of permeant ion binding and blocker permeation (Fig. 6), as described in detail previously [11, 15]. Apparent blocker dissociation constant, K_d, was

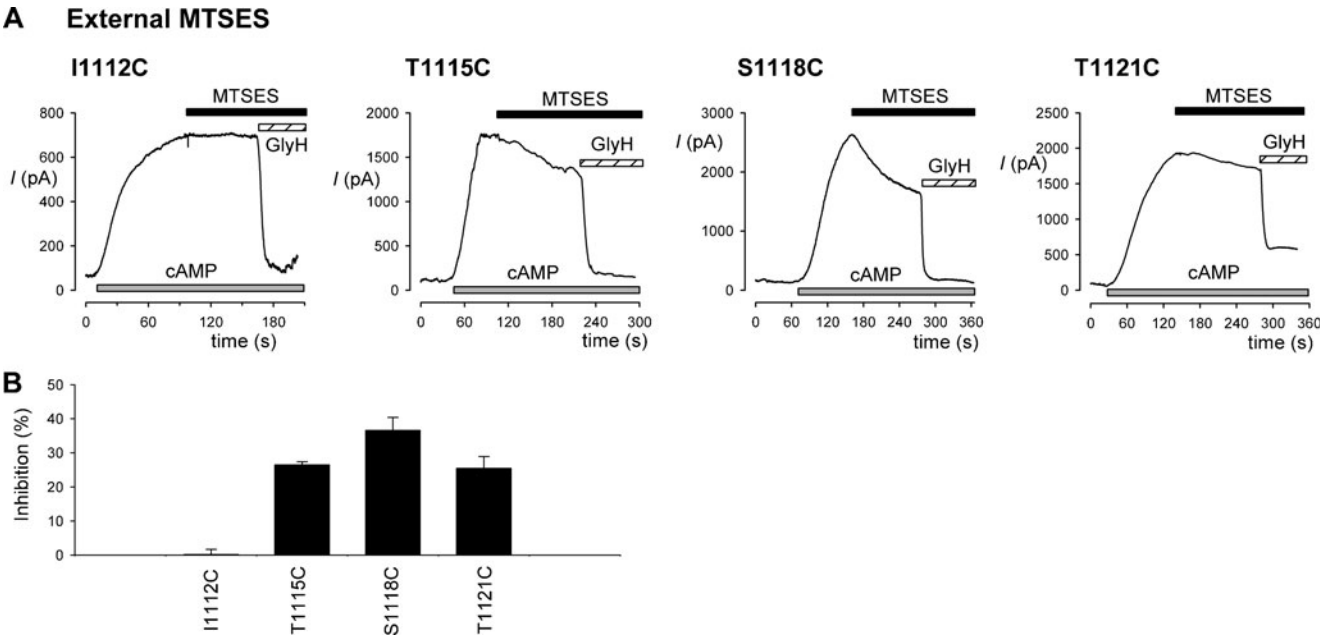

Fig. 3 Modification of cysteine-substituted CFTR-TM11 mutants by external MTSES. **a** Example whole cell currents recorded continuously at +30 mV for the same four TM11 mutants shown in Fig. 2a. CFTR currents were activated by application of cAMP stimulatory cocktail (indicated as cAMP, *gray bars*) and subsequently treated with external MTSES (200 μM, *black bars*) followed by the specific CFTR inhibitor GlyH-101 (50 μM, *hatched bars*). Lack of effect of external MTSES on cys-less CFTR under identical conditions was shown recently [42]. **b** Mean effect of external MTSES on these TM11 cysteine mutants. *Black bars* represent a significant difference from cys-less ($P<0.05$); *gray bars* (I1112C only) no significant difference. Mean of data from three to six patches

approximated from:

$$K_d = \left[Au(CN)_2^-\right] \Big/ \left(\left[1 \Big/ \left(I \Big/ I_0\right)\right] - 1\right)$$

where I is the current amplitude measured following the addition of $Au(CN)_2^-$ and I_0 is the control, unblocked current amplitude.

T338A, as well as other substitutions at this position, cause complex changes in the relative permeability of different anions in CFTR [26]; however, the major changes observed in T338A can be summarized as (a) an increase in the relative permeability of lyotropic anions such as SCN^-, NO_3^-, Br^-, I^-, and ClO_4^-, and (b) an increase in the relative permeability of extracellular organic (kosmotropic) monvalent anions including formate, acetate, propanoate, and pyruvate [26]. These effects probably reflect the roles of ion dehydration and steric factors, respectively, in determining the permeability of different anions in the CFTR channel [23, 26]. To investigate and exemplify these different effects in a simple fashion, we have studied the relative permeability of intracellular SCN^- (Fig. 7) [14, 26] and extracellular acetate (Fig. 8; due to the different observed permeability of organic anions when present in the intracellular or extracellular solution [23, 26]). For experiments involving both SCN^- and acetate-containing solutions, the macroscopic current reversal potential (V_{REV}) was estimated by fitting a polynomial function to the leak-subtracted current–voltage relationship and used to calculate the relative permeability of these anions relative to that of Cl^- (P_{SCN}/P_{Cl} or $P_{acetate}/P_{Cl}$) according to:

$$V_{REV} = \left(RT \Big/ F\right) \ln\left[\left(P_{SCN}[SCN^-]_{in} + P_{Cl}[Cl^-]_{in}\right) \Big/ \left(P_{Cl}[Cl^-]_{out}\right)\right]$$

where $[SCN^-]_{in}$=150 mM, $[Cl^-]_{in}$=4 mM, and $[Cl^-]_{out}$=154 mM or:

$$V_{REV} = \left(RT \Big/ F\right) \ln\left[\left(P_{Cl}[Cl^-]_{in}\right) \Big/ \left(P_{acetate}[acetate]_{out} + P_{Cl}[Cl^-]_{out}\right)\right]$$

where $[Cl^-]_{in}$=154 mM, $[acetate]_{out}$=150 mM, and $[Cl^-]_{out}$=4 mM.

Experiments were carried out at room temperature, 21–24 °C. Values are presented as mean±SEM. Tests of significance were carried out using Student's two-tailed t test. All chemicals were from Sigma-Aldrich (Oakville, ON, Canada) except for GlyH-101 (EMD Chemicals, Gibbstown, NJ, USA), MTSES (Toronto Research Chemicals, North York, ON, Canada), and PKA (Promega, Madison, WI, USA).

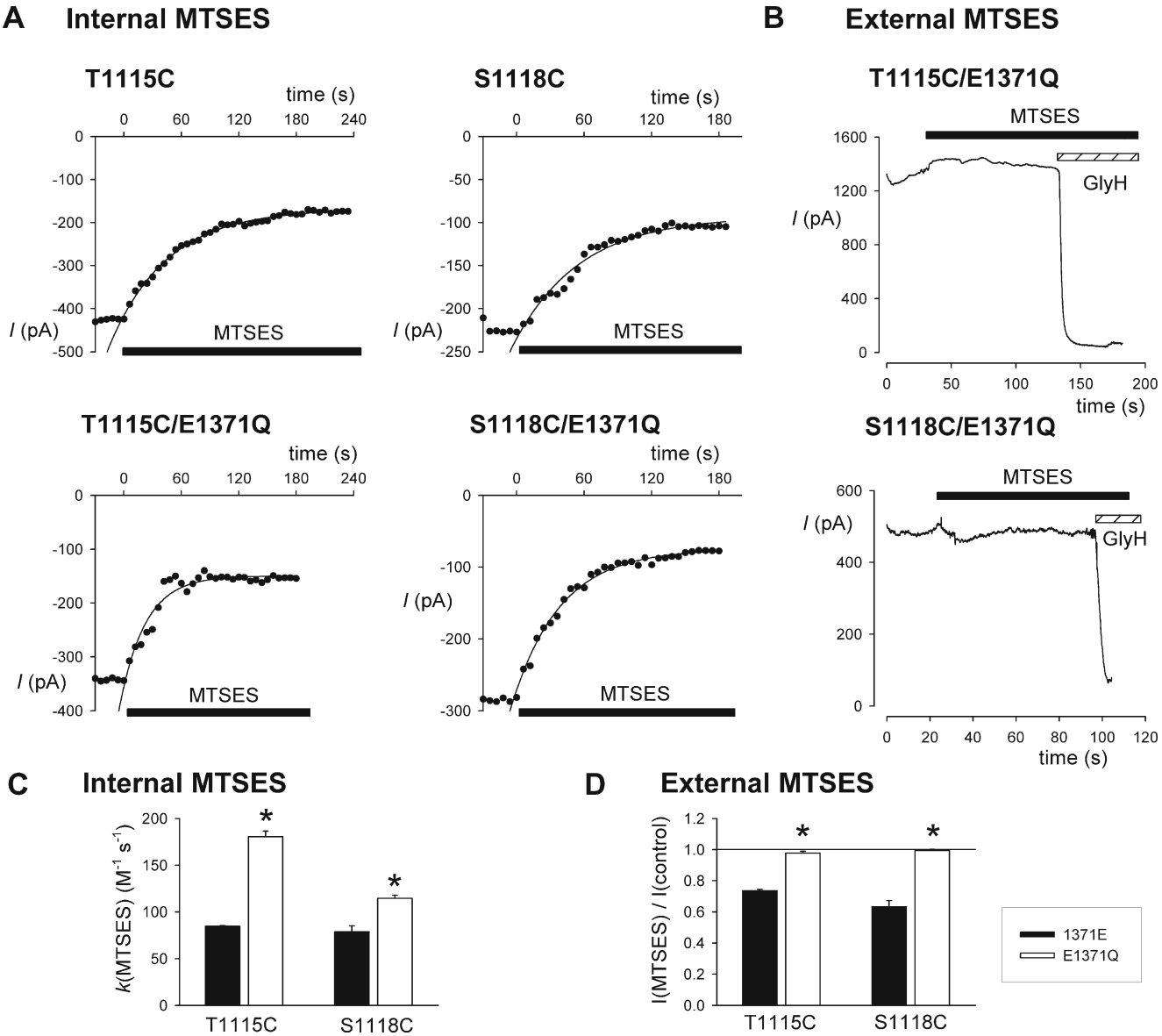

Fig. 4 Effect of the E1371Q mutation on modification by internal and external MTSES. **a** Example time courses of macroscopic currents (measured at −50 mV during voltage ramps) carried by different channel variants in inside-out membrane patches. In each panel, 200 μM MTSES was applied to the cytoplasmic face of the patch at time zero (*black bars*). The decline in current amplitude following MTSES application has been fitted by a single exponential function. **b** Example whole cell currents recorded continuously at +30 mV for constitutively active T1115C/E1371Q and S1118C/E1371Q channels. In contrast to currents carried by T1115C and S1118C channels (see Fig. 3), these whole cell currents were not significantly affected by addition of 200 μM MTSES to the extracellular solution (*black bars*), even though these currents were positively identified as being carried by CFTR by sensitivity to GlyH-101 (50 μM, *hatched bars*). **c** Average modification rate constants (*k*) for MTSES, calculated from fits to data such as those shown in **a** as described in the "Materials and methods" section. **d** Average extent of MTSES inhibition of whole cell current amplitude following 2 min MTSES application, calculated from data such as shown in **b** and Fig. 3. In both **c** and **d**, *black bars* represent the named mutants in a cys-less background, and *white bars* in a cys-less/E1371Q background, and *asterisks* indicate a significant difference between these two backgrounds ($P<0.05$). Mean of data from three to six patches

Results

Accessibility of cysteine side chains introduced into TMs 5, 7, and 11

We hypothesized that the central portion of the CFTR pore might be lined by TMs 1, 5, 6, 7, 11, and 12 (Fig. 1). Previously, we used internal application of MTSES to identify pore-lining cysteine side chains introduced into TM1 [44], TM6 [8], and TM12 [34] of cys-less CFTR. In the present work, we have extended this approach to parts of TMs 5, 7, and 11, selected by alignment with key residues in TMs 1, 6, and 12 (Fig. 1). Figure 2a shows the effect of internal MTSES on currents carried by some TM11 mutant channels in inside–

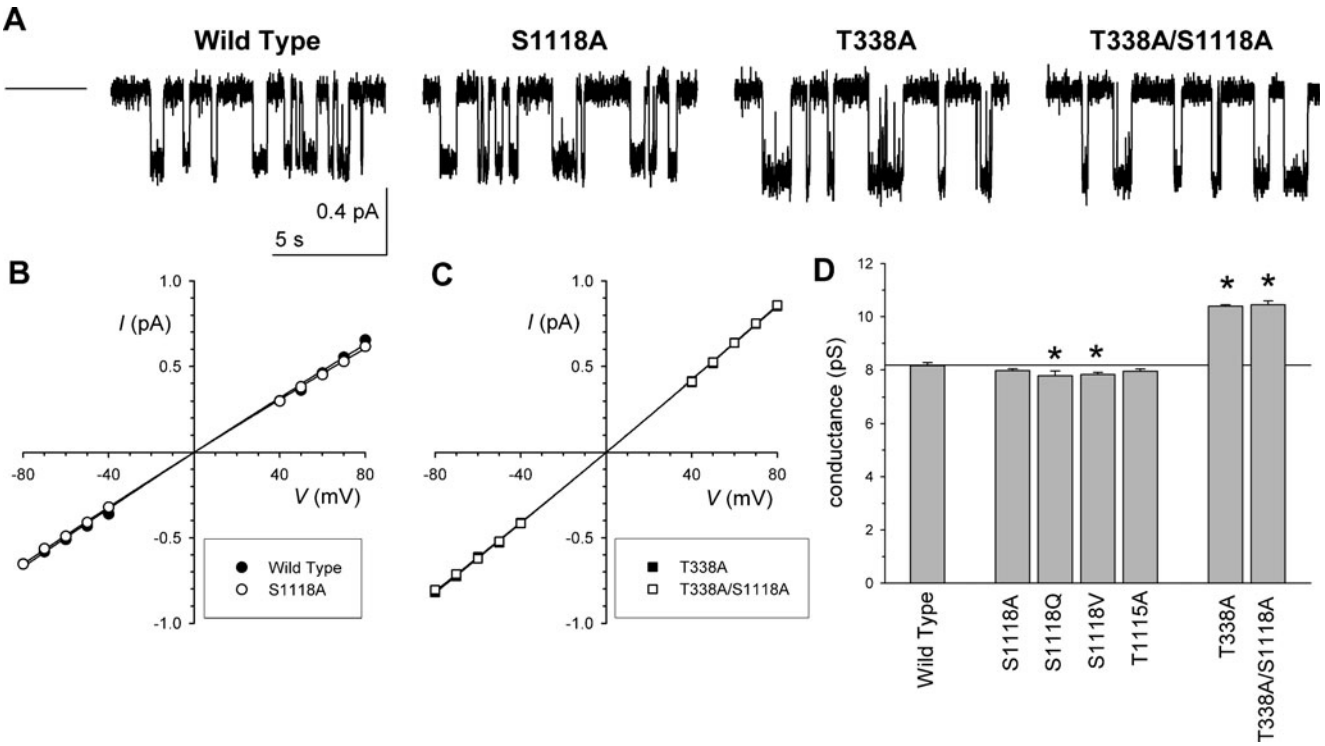

Fig. 5 Single channel currents carried by TM11 mutant channels. **a** Example single channel currents carried by the named channel variants at a membrane potential of −50 mV. The *horizontal line to the left of the traces* indicates the channel closed state current level. **b**, **c** Mean single channel *I–V* relationships for these channel variants. **d** Mean single channel conductance measured from the slope of individual *I–V* relationships. *Asterisks* indicate a significant difference from wild type ($P<0.05$). Mean of data from 6 to 12 patches in **b**–**d**

out membrane patches during voltage ramps, and Fig. 2b shows the timecourse of current change monitored at −50 mV in these same membrane patches. Application of MTSES (200 μM) following channel activation with PKA and ATP caused a decrease in macroscopic current amplitude in I1112C, T1115C and S1118C, but not in T1121C (Fig. 2a, b) or in I1109C, F1110C, F1111C, A1113C, V1114C, F1116C, or I1117C (Fig. 2c). In contrast to these results indicating modification of cysteine side chains introduced into TM11 by internal MTSES, we found no evidence for modification of cysteine side chains introduced into TM5 or TM7. Thus, although ATP- and PKA-dependent, $CFTR_{inh}$-172-sensitive macroscopic currents were observed for several cysteine mutants in TM5 and TM7, in no case were these currents significantly affected by internal application of 200 μM MTSES (Fig. 2c). We did not observe any CFTR current in inside-out patches associated with E873C (TM7). These preliminary experiments therefore do not support an important role for either TM5 or TM7 in forming the inner vestibule or central portion of the CFTR pore.

Previously it was shown that S1118C, T1121C, and T1122C—but not F1116C, I1117C, I1119C, or L1120C—are accessible to externally applied MTS reagents [10]. Figure 3 confirms that application of external MTSES (200 μM) following channel activation with cAMP-stimulatory cocktail caused a decrease in whole cell current amplitude in T1115C, S1118C, and T1121C, but not in I1112C. Together, these results (Figs. 2b, 3b) suggest that S1118C represents the outermost extent of internal MTSES penetration into the pore, and T1115 the innermost extent of external MTSES penetration. Interestingly, the central portion of TM11 including the pore-accessible side chains of T1115 and S1118, is accessible to MTSES reagents applied to either side of the membrane. This dual accessibility is common with some residues in TM6 [8] but contrasts with TMs 1 and 12, in which no side chains were found to be accessible to both internal and external MTS reagents [34, 44].

State-dependent accessibility of T1115C and S1118C in TM11

Modification of T1115C and S1118C by both internal and external MTSES is reminiscent of the accessibility pattern observed for TM6 cysteine mutant T338C [42]. This similarity is perhaps not surprising since a disulfide bond can be formed between the two cysteine side chains of T338C and S1118C in open channels [43], indicating close physical proximity of these pore-exposed side chains. Previously we suggested that the ability of T338C to be modified by MTSES from both sides of the membrane was due to this residue

showing alternate access during channel gating, being accessible from the outside in closed channels and from the inside in open channels [42]. This suggestion was based in large part on the effects of the E1371Q mutation, which results in constitutively open CFTR channels, on side-dependent modification. As shown in Fig. 4a, c, the E1371Q mutation significantly accelerated the rate of modification of both T1115C and S1118C by intracellular MTSES, suggesting that these cysteines are more readily modified from the inside in open channels. In contrast, these channels bearing the E1371Q mutation were almost completely insensitive to external MTSES (Fig. 4b), suggesting that these cysteines are much more difficult to modify from the outside in open channels (Fig. 4d). These results suggest that, much like T338 in TM6 [42], TM11 residues T1115 and S1118 move from a relatively externally accessible location in closed channels to a relatively internally accessible location in open channels.

Comparison of the roles of T338 and S1118 in determining the functional properties of the CFTR pore

The cysteine accessibility results described above suggest that TM11 residues T1115 and S1118 occupy a similar location within the pore as that of TM6 residue T338. This suggestion is consistent with data that S1118C can form a disulfide bond with T338C in open channels [43]. T338 is thought to be located close to the narrowest part of the CFTR open channel pore, since mutations at this site have a variety of effects on channel permeation properties that are correlated with the side chain volume of the introduced amino acid (see the "Introduction" section). We therefore carried out a

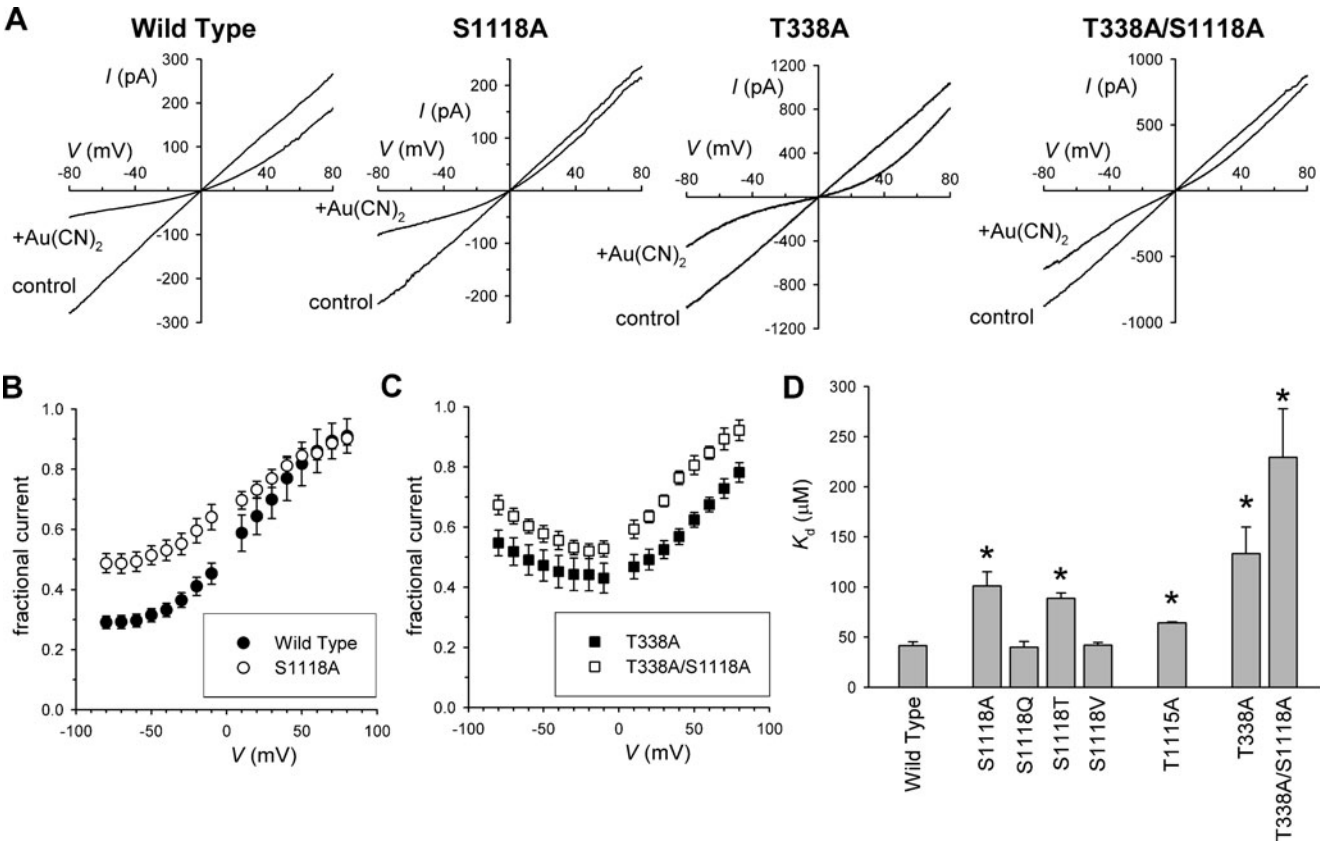

Fig. 6 Block of macroscopic currents by internal $Au(CN)_2^-$ ions. **a** Example leak-subtracted *I–V* relationships for different CFTR variants in inside–out patches. In each case currents were recorded before (control) and after addition of 100 μM Au $(CN)_2^-$ to the intracellular solution. **b**, **c** Mean fractional current remaining following addition of this concentration of $Au(CN)_2^-$ as a function of voltage. **d** Mean K_d (at −80 mV), calculated from data such as that shown in **b** and **c** as described in the "Materials and methods" section. *Asterisks* indicate a significant difference from wild type ($P<0.02$). Mean of data from 3 to 8 patches in **b**–**d**

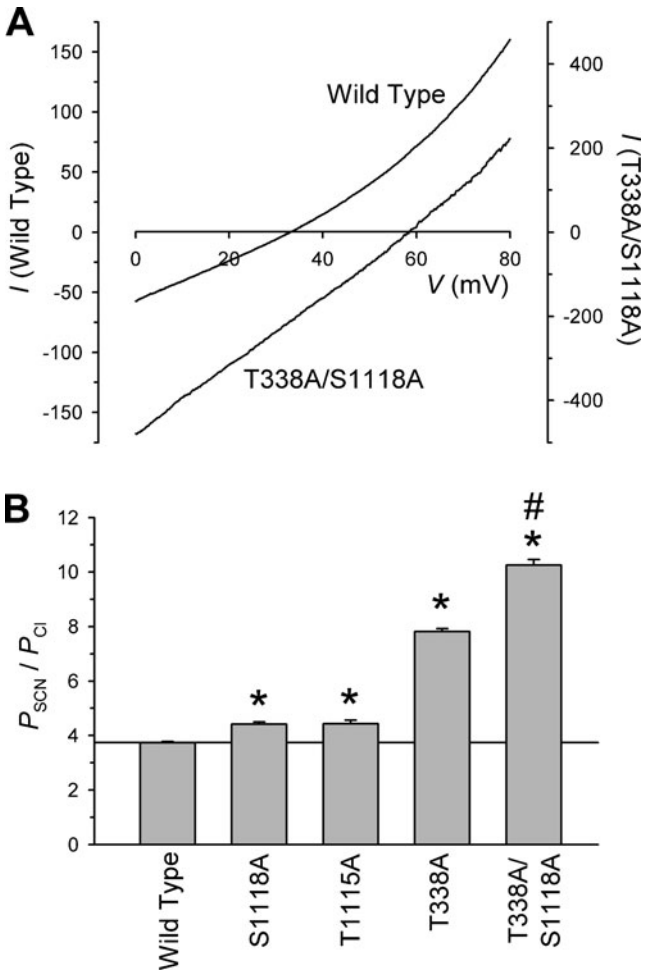

Fig. 7 Thiocyanate permeability of mutants. **a** Example leak-subtracted *I–V* relationships (from two different patches) recorded with Cl^--containing extracellular solutions and SCN^--containing intracellular solutions. The depolarizing (*rightward*) shift in the current reversal potential indicates an increased P_{SCN}/P_{Cl} in the T338A/S1118A double mutant. **b** Mean P_{SCN}/P_{Cl} values calculated from reversal potential measurements under these conditions as described in the "Materials and methods" section. Mean of data from three to six patches. *Asterisks* indicate a significant difference from wild type ($P<0.01$), while *hashtag* indicates a significant difference from the T338A mutant ($P<0.0002$)

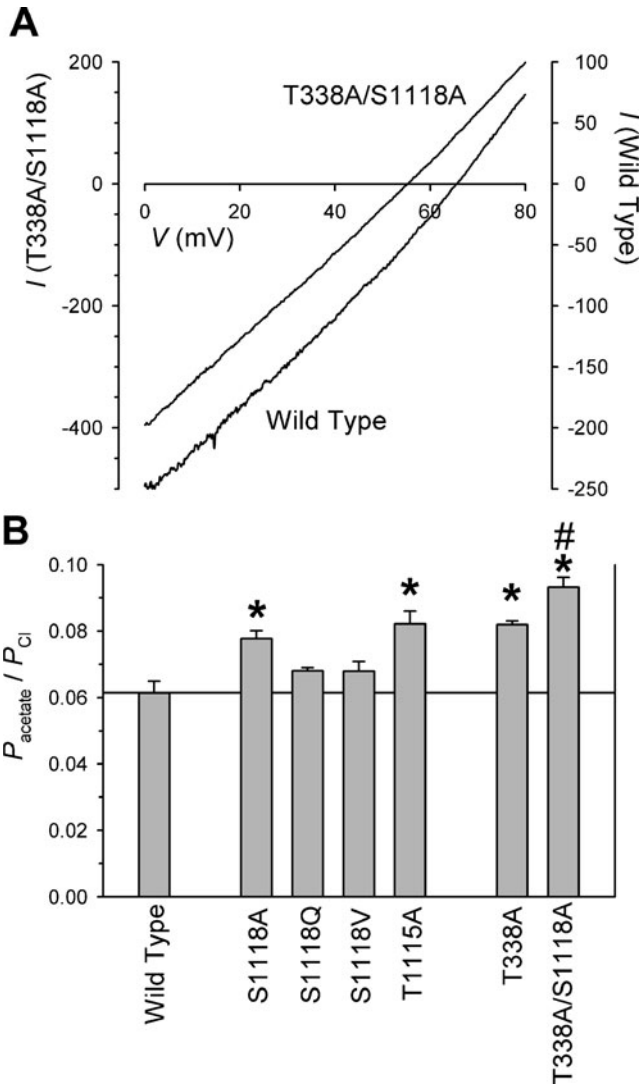

Fig. 8 Acetate permeability of mutants. **a** Example leak-subtracted *I–V* relationships (from two different patches) recorded with Cl^--containing intracellular solutions and acetate-containing extracellular solutions. The hypolarizing (*leftward*) shift in the current reversal potential indicates an increased $P_{acetate}/P_{Cl}$ in the T338A/S1118A double mutant. **b** Mean $P_{acetate}/P_{Cl}$ values calculated from reversal potential measurements under these conditions as described in the "Materials and methods" section. Mean of data from three to five patches. *Asterisks* indicate a significant difference from wild type, while *hashtag* indicates a significant difference from the T338A mutant ($P<0.01$)

series of experiments designed to investigate if S1118 might play a similar functional role within the pore as that proposed for T338. In addition, possible additive effects of reducing the side chain volumes of these two nearby residues was investigated using a T338A/S1118A double mutant. These experiments, carried out in a wild-type CFTR background, were designed to provide a simple test of the relative effects of mutations on (a) single channel conductance (Fig. 5), (b) open channel block by permeant anions (Fig. 6), (c) lyotropic anion selectivity (Fig. 7), and (d) permeation of large organic anions (Fig. 8) - channel functional properties that have previously been shown to be sensitive to mutation of T338 (see the "Introduction" section).

Previously it was shown that the S1118C mutation reduced single channel conductance at depolarized membrane potentials [10]. In contrast, S1118A had no effect on conductance, while S1118Q and S1118V were associated with

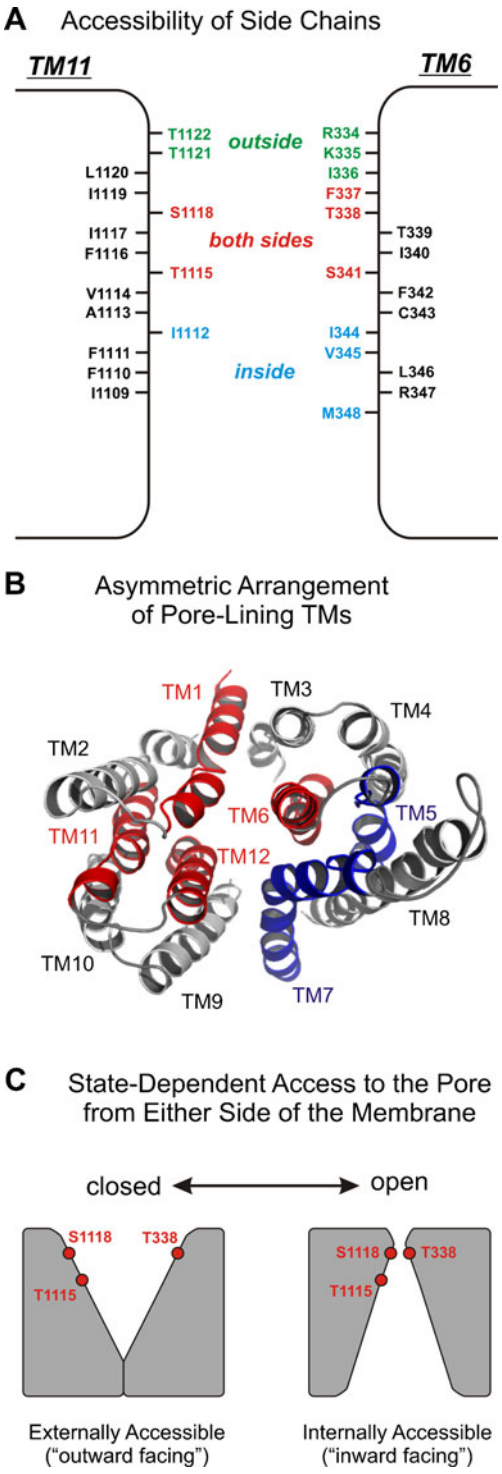

Fig. 9 Model of TM contributions to the pore in open and closed CFTR channels. **a** Proposed locations of pore-lining side chains in TM11 (*left*) and TM6 (*right*). TM11 residues that were modified by MTSES applied to either side of the membrane (T1115, S1118) are shown in *red*. Based on evidence from Figs. 2 and 3, and previous work using external MTS reagents [10], residues that were modified only by internal MTSES are shown in *blue* and those modified only by external MTS reagents in *green*, while residues for which no evidence for modification has been obtained are in *black*. This pattern of MTS sensitivity is compared to previously published work from TM6 [8]; similar alignments with TMs 1 and 12 have also previously been presented [34]. **b** Position of pore-lining TMs in the atomic homology model of Fig. 1. Different TMs are visualized from the extracellular side of the membrane. Putative pore-lining TMs 1, 6, 11, and 12 are shown in *red*, with non-pore-lining TMs 5 and 7 in *blue*. **c** Proposed changes in orientation of TM11 residues T1115 and S1118 during channel gating. As proposed previously for TM6 residue T338 [42], the channel is shown as being in an "outward facing" configuration when closed (with T1115 and S1118 accessible from the outside), and switching to an "inward facing" configuration on opening (with T1115 and S1118 accessible from the inside)

very small (<5 %) reductions in conductance (Fig. 5). Conductance was also unaltered in T1115A. In each case, the single channel *I–V* relationship remained linear (e.g., Fig. 5-b), in contrast to the strongly inwardly rectified *I–V* relationship previously observed for S1118C [10]. These very minor effects on conductance are in contrast with the large (>25 %) increase seen in T338A (Fig. 5), as reported previously [26]. The double mutant T338A/S1118A had a similarly elevated conductance that was not significantly different from that of T338A alone ($P>0.75$; Fig. 5).

Altered movement of permeant ions in the pore of T338A-CFTR is also reflected by changes in the voltage-dependent block of Cl^- currents by low concentrations of permeant $Au(CN)_2^-$ ions [11, 14, 15]. As shown in Fig. 6, channel block by intracellular $Au(CN)_2^-$ ions is altered in two distinct ways by the T338A mutation: (a) block is significantly weakened and (b) the *I–V* relationship in the presence of $Au(CN)_2^-$ shows an unusual "N"-shape (Fig. 6a), resulting in a "U"-shaped fractional current–voltage relationship (Fig. 6c) that indicates strongest block close to 0 mV membrane potential that is weakened at both more hyperpolarized and more depolarized voltages. This unusual shape is thought to reflect increased unblock by blocker permeation at hyperpolarized voltages, which may reflect a reduced barrier to $Au(CN)_2^-$ movement inside the pore in T338A [11]. Block by intracellular $Au(CN)_2^-$ was also significantly weakened in S1118A, S1118T, and T1115A compared to wild type, especially at hyperpolarized membrane potentials (Fig. 6); however, no apparent "U"-shape to the fractional current–voltage relationship was observed (Fig. 6b). Interestingly, block of the T338A/S1118A double mutant was slightly weaker than for T338A alone (Fig. 6c, d), suggesting that these two mutations might have additive effects on $Au(CN)_2^-$ binding in the pore. As observed at the single channel level (Fig. 5), the macroscopic *I–V* relationships for all mutants remained linear (e.g., Fig. 6a), in contrast to the strongly inwardly rectifying relationship previously observed for S1118C [10].

Changes in lyotropic anion selectivity were determined by estimating SCN^- permeability from macroscopic current reversal potential measurements with SCN^--containing bath solutions [10, 14] (Fig. 7). Under these conditions, SCN^- permeability was slightly but significantly increased in both

S1118A and T1115A, although this increase was much less than that observed in T338A (Fig. 7b). Interestingly, SCN^- permeability was further increased in the T338A/S1118A double mutant (Fig. 7). Changes in the permeability of organic anions, the permeability of which are limited by steric factors at the narrowest part of the pore [25], were determined from macroscopic current reversal potential measurements with acetate-containing pipette solutions [26] (Fig. 8). Acetate permeability was slightly increased in S1118A and T1115A, but not significantly changed in S1118Q or S1118V (Fig. 8b). Again, the increase in acetate permeability seen in T338A was significantly augmented in the T338A/S1118A mutation (Fig. 8), suggesting an additive effect of these two mutations on organic anion permeability.

Discussion

Our present results, combined with those presented earlier concerning MTS accessibility from the extracellular side of the membrane [10], suggest that TM11 lines the CFTR pore and can be divided into regions that are accessible to large MTS reagents from the cytoplasmic side of the membrane only, from the extracellular side only, or from either side of the membrane. The pattern of accessibility for TM11 is summarized and compared to the pattern observed in TM6 [8] in Fig. 9a; we have also previously presented similar schemes for TM1 [44] and TM12 [34]. The proposed relative alignment of TMs 6 and 11 presented in Fig. 9a is consistent not only with the pattern of MTSES accessibility from different sides of the membrane, but also with previous data showing that disulfide bonds can form between T338C and S1118C, and between R334C and T1122C, in open channels [43].

Substituted cysteine accessibility mutagenesis experiments therefore suggest that the CFTR pore is lined by TMs 1, 6, 11, and 12, and that residues in each of these TMs are accessible either to the extracellular or the intracellular solution ([2–4, 8, 10, 13, 33, 34, 44] and present results); this SCAM data is consistent with structure–function analyses that suggest that these TMs make the most important functional contributions to the pore [18, 21, 28]. In contrast, our present results using similar techniques provide no evidence for accessibility of side chains in TMs 5 or 7 to intracellular MTSES (Fig. 2), suggesting that these TMs may not line the pore, at least over the (approximately central) parts of these TMs investigated (Fig. 1). It is possible that other TMs may contribute to the lining of the pore, for example TMs 3 and/or 9 [1, 33], and also that the relative contribution of different TMs may change at different locations along the axis of the pore [33, 44]. For example, R303 at the cytoplasmic end of TM5 has been shown to contribute to the inner mouth of the pore [39, 40]. Other kinds of ion channels with multi-subunit structures in which different subunits make quite symmetrical contributions to the channel pore typically have pores that are lined by between four and six TM regions [16]. The CFTR channel is formed by a single subunit but is still thought to have a two-fold symmetrical structure due to its two homologous groups of six TMs; in fact, the TMs are thought to be arranged in two symmetrical wings, one made up of TMs 1, 2, 9, 10, 11, 12, and the other TMs 3, 4, 5, 6, 7, 8 (see the "Introduction" section). Taking the idea that the CFTR pore is lined by TMs 1, 6, 11, and 12 at face value would suggest that the pore is in fact not symmetrical—whereas "mirror-image" TMs 6 and 12 both contribute to the pore (albeit asymmetrically—see [34]) the contributions of TMs 1 and 11 are apparently not matched by their "mirror-image" TMs 7 and 5 (Fig. 9b). Furthermore, of the four apparent pore-lining TMs, three are in one "wing" (TMs 1, 11, and 12) with only TM6 coming from the other, structurally supposedly symmetrical wing (Fig. 9b). This apparent asymmetry in the CFTR pore should be taken into account when modeling the structure of CFTR on other, clearly symmetrical ABC proteins.

Two side chains in TM11–T1115 and S1118 - are accessible to large MTSES reagents applied either to the extracellular or the intracellular side of the membrane (Figs. 2, 3, and 9). This is in common with F337, T338, and S341 in TM6 [8] (Fig. 9a) but in contrast to TMs 1 and 12, where no residues were found to show accessibility to both sides of the membrane [34, 44]. Furthermore, using the same approach used previously to study side-dependent modification of T338C [42], we found that T1115C and S1118C were more readily modified from the extracellular solution in closed channels, but more readily modified from the intracellular solution in open channels (Fig. 4). This pattern, which is common to that previously observed for T338C [42], is consistent with these residues showing alternating access to the extracellular and intracellular sides of the membrane during channel opening and closing (Fig. 9c). In this scheme, channel opening and closing is controlled by a cytoplasmic gate [41], with the outer part of the pore (close to T338, T1115, and S1118) paradoxically narrowing when the channel opens [43]. This scheme puts T338 and S1118 close to the narrowest part of the open channel pore (Fig. 9c), and is consistent with the finding that cysteines introduced at these two positions can form disulfide bonds only in the channel open state [43], since these two residues are proposed to move closer together when the channel opens and to move further apart when the channel closes (Fig. 9c). The similar apparent changes in accessibility of residues in TMs 6 and 11 during channel gating (Fig. 9c), in contrast to the finding that residues in TMs 1 and 12 do not show such dramatic changes in accessibility relative to the membrane [34, 44], suggests that TMs 6 and 11 may show similar movements during channel opening and closing.

Longstanding functional evidence also suggests that T338 is located close to the narrowest part of the open channel pore (see the "Introduction" section). The idea that the side chains of T338 and S1118 are situated close together in open channels (Fig. 9c) therefore suggests that S1118 may also contribute to the functional properties of the narrow pore region, and further that co-mutagenesis of T338 and S1118 may have the potential to lead to larger changes in the functional diameter of the narrow pore lumen. However, mutagenesis of S1118 to residues with smaller (alanine) or larger (glutamine, valine) residues had surprisingly small effects on channel functional properties, in particular compared to those of mutagenesis of T338A. The effects of the S1118A mutation on permeant anion ($Au(CN)_2^-$) binding (Fig. 6), permeability of the lyotropic SCN^- anion (Fig. 7), and permeability of the organic acetate anion (Fig. 8) were qualitatively similar to, but generally smaller than, those of T338A, and in fact similar effects were seen in T1115A. Neither S1118A nor T1115A significantly altered single channel conductance, although introduction of larger amino acid side chains in S1118Q and S1118V led to very small decreases in conductance (Fig. 5). Previously, it was shown that substitution of S1118 with a much larger phenylalanine residue (S1118F) caused a larger (~35 %) decrease in single channel conductance [46]. Mutagenesis of T338 to residues with a larger side chain volume (asparagine, isoleucine, valine) leads to a dramatic (>90 %) decrease in conductance [26]. Reduction of side chain volume in S1118A and T1115A, like T338A, led to an increase in the relative permeability of the small organic anion acetate, consistent with an increase in the apparent diameter of the narrowest region of the pore [25, 26]; however, introduction of side chains with larger volume (S1118Q, S1118V) did not lead to a decrease in acetate permeability (Fig. 8). Together these results suggest only very minor functional roles for S1118 and T1115 that are difficult to correlate with changes in side chain volume. Simultaneous mutagenesis of T338 and S1118 to small alanine residues also had only small additional effects compared to the T338A mutation alone (Figs. 5, 6, 7, and 8). Most striking here were a significantly increased permeability of the T338A/S1118A double mutant both to SCN^- (Fig. 7) and to acetate (Fig. 8). Permeability of small lyotropic anions like SCN^- might be influenced by interactions throughout the pore [18, 38] or might be determined predominantly at a localized "selectivity filter" [18, 24] and so the apparently additive effects of the T338A and S1118A mutations is difficult to interpret in terms of the relative roles or locations of these two residues. Permeability of large anions such as acetate is thought to be determined predominantly by steric factors at the narrowest part of the pore [25], and so the increase in acetate permeability in T338A/S1118A compared to either mutation alone might be considered evidence that these two mutations impact the dimensions of a common, narrow region of the pore. One possible reason contributing to the minor functional effects observed in these experiments is that S1118A (and T1115A) might be considered relatively conservative mutations leading to only small changes in amino acid side chain volume. Nevertheless, T338A (which results in a similarly small reduction in side chain volume) is associated with much greater changes in pore properties. Previously, the S1118C mutation was shown to decrease conductance at positive voltages, leading to inward rectification of both the single channel and macroscopic current–voltage relationships [10], and although this would be considered a very conservative mutation (one oxygen atom replaced by sulfur) this effect was not reproduced in S1118A, S1118Q or S1118 (Fig. 5). Given that the effects of the S1118C mutation on single channel conductance and rectification were exacerbated by modification by external MTSES, and mostly reversed by modification with positively charged MTSET [10], these effects might reflect partial negative charge of the introduced cysteine side chain rather than a change in side chain volume.

Conclusions

Overall TM11 and TM6 appear to make broadly similar contributions to the lining of the CFTR pore (Fig. 9a) and to undergo similar conformational rearrangements during channel opening and closing (Fig. 9c). However, these two TMs appear to make different functional contributions to the narrow region of the pore, as evidenced by the relatively minor functional effects of mutation of S1118 compared to T338. While these data are consistent with longstanding evidence that TM6 plays a dominant role in determining the functional properties of the pore [18, 21, 28], it remains unclear why one TM apparently dominates the functional properties of a three-dimensional structure such as the narrow pore region. Furthermore, comparison of different TMs using a common SCAM approach suggests an asymmetric overall pore structure, casting some questions over the supposed symmetric structural arrangement of the TMs (Fig. 9b).

Acknowledgments This work was supported by the Canadian Institutes of Health Research and Cystic Fibrosis Canada (CFC). Wuyang Wang and Yassine El Hiani were supported by CFC postdoctoral fellowships.

References

1. Akabas MH (1998) Channel-lining residues in the M3 membrane-spanning segment of the cystic fibrosis transmembrane conductance regulator. Biochemistry 37:12233–12240

2. Alexander C, Ivetac A, Liu X, Norimatsu Y, Serrano JR, Landstrom A, Sansom M, Dawson DC (2009) Cystic fibrosis transmembrane conductance regulator: using differential reactivity toward channel-permeant and channel-impermeant thiol-reactive probes to test a molecular model for the pore. Biochemistry 48:10078–10088
3. Bai Y, Li M, Hwang T-C (2010) Dual roles of the sixth transmembrane segment of the CFTR chloride channel in gating and permeation. J Gen Physiol 136:293–309
4. Bai Y, Li M, Hwang T-C (2011) Structural basis for the channel function of a degraded ABC transporter, CFTR (ABCC7). J Gen Physiol 138:495–507
5. Beck EJ, Yang Y, Yaemsiri S, Raghuram V (2008) Conformational changes in a pore-lining helix coupled to cystic fibrosis transmembrane conductance regulator channel gating. J Biol Chem 283:4957–4966
6. Cui G, Song B, Turki HW, McCarty NA (2012) Differential contribution of TM6 and TM12 to the pore of CFTR identified by three sulfonylurea-based blockers. Pflügers Arch 463:405–418
7. Dalton J, Kalid O, Schushan M, Ben-Tal N, Villà-Freixa J (2012) New model of cystic fibrosis transmembrane conductance regulator proposes active channel-like conformation. J Chem Inf Model 52:1842–1853
8. El Hiani Y, Linsdell P (2010) Changes in accessibility of cytoplasmic substances to the pore associated with activation of the cystic fibrosis transmembrane conductance regulator chloride channel. J Biol Chem 285:32126–32140
9. El Hiani Y, Linsdell P (2012) Tuning of CFTR chloride channel function by location of positive charges within the pore. Biophys J 103:1719–1726
10. Fatehi M, Linsdell P (2009) Novel residues lining the CFTR chloride channel pore identified by functional modification of introduced cysteines. J Membr Biol 228:151–164
11. Fatehi M, St. Aubin CN, Linsdell P (2007) On the origin of asymmetric interactions between permeant anions and the CFTR chloride channel pore. Biophys J 92:1241–1253
12. Gadsby DC, Vergani P, Csanády L (2006) The ABC protein turned chloride channel whose failure causes cystic fibrosis. Nature 440:477–483
13. Gao X, Bai Y, Hwang T-C (2013) Cysteine scanning of CFTR's first transmembrane segment reveals its plausible roles in gating and permeation. Biophys J 104:786–797
14. Ge N, Muise CN, Gong X, Linsdell P (2004) Direct comparison of the functional roles played by different transmembrane regions in the cystic fibrosis transmembrane conductance regulator chloride channel pore. J Biol Chem 279:55283–55289
15. Gong X, Burbridge SM, Cowley EA, Linsdell P (2002) Molecular determinants of $Au(CN)_2^-$ binding and permeability within the cystic fibrosis transmembrane conductance regulator Cl^- channel pore. J Physiol 540:39–47
16. Hille B (2001) Ion Channels of Excitable Membranes, 3rd edn. Sinauer Associates, Sunderland
17. Hunt JF, Wang C, Ford RC (2013) Cystic fibrosis transmembrane conductance regulator (ABCC7) structure. Cold Spring Harb Perspect Med 3:a009514
18. Hwang T-C, Kirk KL (2013) The CFTR ion channel: gating, regulation, and anion permeation. Cold Spring Harb Perspect Med 3:a009498
19. Hwang T-C, Sheppard DN (1999) Molecular pharmacology of the CFTR Cl^- channel. Trends Pharmacol Sci 20:448–453
20. Li M-S, Demsey AFA, Qi J, Linsdell P (2009) Cysteine-independent inhibition of the CFTR chloride channel by the cysteine-reactive reagent sodium (2-sulfonatoethyl) methanethiosulfonate (MTSES). Brit J Pharmacol 157:1065–1071
21. Linsdell P (2006) Mechanism of chloride permeation in the cystic fibrosis transmembrane conductance regulator chloride channel. Exp Physiol 91:123–129
22. Linsdell P (2001) Relationship between anion binding and anion permeability revealed by mutagenesis within the cystic fibrosis transmembrane conductance regulator chloride channel pore. J Physiol 531:51–66
23. Linsdell P, Hanrahan JW (1998) Adenosine triphosphate-dependent asymmetry of anion permeation in the cystic fibrosis transmembrane conductance regulator chloride channel. J Gen Physiol 111:601–614
24. Linsdell P, Evagelidis A, Hanrahan JW (2000) Molecular determinants of anion selectivity in the cystic fibrosis transmembrane conductance regulator chloride channel pore. Biophys J 78:2973–2982
25. Linsdell P, Tabcharani JA, Rommens JM, Hou Y-X, Chang X-B, Tsui L-C, Riordan JR, Hanrahan JW (1997) Permeability of wild-type and mutant cystic fibrosis transmembrane conductance regulator chloride channels to polyatomic anions. J Gen Physiol 110:355–364
26. Linsdell P, Zheng S-X, Hanrahan JW (1998) Non-pore lining amino acid side chains influence anion selectivity of the human CFTR Cl^- channel expressed in mammalian cell lines. J Physiol 512:1–16
27. Lubamba B, Dhooghe B, Noel S, Leal T (2012) Cystic fibrosis: insight into CFTR pathophysiology and pharmacotherapy. Clin Biochem 45:1132–11144
28. McCarty NA (2000) Permeation through the CFTR chloride channel. J Exp Biol 203:1947–1962
29. McCarty NA, Zhang Z-R (2001) Identification of a region of strong discrimination in the pore of CFTR. Am J Physiol 281:L852–L867
30. Mense M, Vergani P, White DM, Altberg G, Nairn AC, Gadsby DC (2006) *In vivo* phosphorylation of CFTR promotes formation of a nucleotide-binding domain heterodimer. EMBO J 25:4728–4739
31. Mornon J-P, Lehn P, Callebaut I (2008) Atomic model of human cystic fibrosis transmembrane conductance regulator: membrane-spanning domains and coupling interfaces. Cell Mol Life Sci 65:2594–2612
32. Mornon J-P, Lehn P, Callebaut I (2009) Molecular models of the open and closed states of the whole human CFTR protein. Cell Mol Life Sci 66:3469–3486
33. Norimatsu Y, Ivetac A, Alexander C, Kirkham J, O'Donnell N, Dawson DC, Sansom MS (2012) Cystic fibrosis transmembrane conductance regulator: a molecular model defines the architecture of the anion conduction path and locates a "bottleneck" in the pore. Biochemistry 51:2199–2212
34. Qian F, El Hiani Y, Linsdell P (2011) Functional arrangement of the 12th transmembrane region in the CFTR chloride channel pore based on functional investigation of a cysteine-less CFTR variant. Pflügers Arch 462:559–571
35. Rosenberg MF, O'Ryan LP, Hughes G, Zhao Z, Aleksandrov LA, Riordan JR, Ford RC (2011) The cystic fibrosis transmembrane conductance regulator (CFTR). Three-dimensional structure and localization of a channel gate. J Biol Chem 286:42647–42654
36. Serohijos AWR, Hegedüs T, Aleksandrov AA, He L, Cui L, Dokholyan NV, Riordan JR (2008) Phenylalanine-508 mediates a cytoplasmic-membrane domain contact in the CFTR 3D structure crucial to assembly and channel function. Proc Natl Acad Sci USA 105:3256–3261
37. Smith SS, Liu X, Zhang Z-R, Sun F, Kriewall TE, McCarty NA, Dawson DC (2001) CFTR: covalent and noncovalent modification suggests a role for fixed charges in anion conduction. J Gen Physiol 118:407–431
38. Smith SS, Steinle ED, Meyerhoff ME, Dawson DC (1999) Cystic fibrosis transmembrane conductance regulator. Physical basis for lyotropic anion selectivity patterns. J Gen Physiol 114:799–818
39. St. Aubin CN, Linsdell P (2006) Positive charges at the intracellular mouth of the pore regulate anion conduction in the CFTR chloride channel. J Gen Physiol 128:535–545
40. St. Aubin CN, Zhou J-J, Linsdell P (2007) Identification of a second blocker binding site at the cytoplasmic mouth of the cystic fibrosis transmembrane conductance regulator chloride channel pore. Mol Pharmacol 71:1360–1368

41. Wang W, Linsdell P (2012) Conformational change opening the CFTR chloride channel pore coupled to ATP-dependent gating. Biochim Biophys Acta 1818:851–861
42. Wang W, Linsdell P (2012) Alternating access to the transmembrane domain of the ATP-binding cassette protein cystic fibrosis transmembrane conductance regulator (ABCC7). J Biol Chem 287:10156–10165
43. Wang W, Linsdell P (2012) Relative movements of transmembrane regions at the outer mouth of the cystic fibrosis transmembrane conductance regulator channel pore during channel gating. J Biol Chem 287:32136–32146
44. Wang W, El Hiani Y, Linsdell P (2011) Alignment of transmembrane regions in the cystic fibrosis transmembrane conductance regulator chloride channel pore. J Gen Physiol 138:165–178
45. Zhang Z-R, Song B, McCarty NA (2005) State-dependent chemical reactivity of an engineered cysteine reveals conformational changes in the outer vestibule of the cystic fibrosis transmembrane conductance regulator. J Biol Chem 280:41997–42003
46. Zhang Z-R, McDonough SI, McCarty NA (2000) Interaction between permeation and gating in a putative pore domain mutant in the cystic fibrosis transmembrane conductance regulator. Biophys J 79:298–313
47. Zhou J-J, Fatehi M, Linsdell P (2008) Identification of positive charges situated at the outer mouth of the CFTR chloride channel pore. Pflügers Arch 457:351–360
48. Zhou Z, Hu S, Hwang T-C (2002) Probing an open CFTR pore with organic anion blockers. J Gen Physiol 120:647–662
49. Zhou J-J, Li M-S, Qi J, Linsdell P (2010) Regulation of conductance by the number of fixed positive charges in the intracellular vestibule of the CFTR chloride channel pore. J Gen Physiol 135:229–245